Supporting Information

Structure and Dynamics of Stacking Interactions in an Antibody Binding Site

Ramkrishna Adhikary,[†] Jörg Zimmermann,[†] Robyn L. Stanfield,[‡] Ian A. Wilson,[‡] Wayne Yu,[†] Masayuki Oda,[§] and Floyd E. Romesberg[†]*

[†]Department of Chemistry, [‡]Department of Integrative Structural and Computational Biology and The Skaggs Institute for Chemical Biology, The Scripps Research Institute, La Jolla, CA 92037
[§]Graduate School of Life and Environmental Sciences, Kyoto Prefectural University, 1-5, Hangi-cho, Shimogamo, Sakyo-ku, Kyoto 606-8522, Japan

Supplemental Methods and Discussion

3PEPS and Transient Grating Spectroscopy. The 3PEPS setup has been described in detail previously.[1, 2] Briefly, the output pulses (150 μJ at 836 nm) from a Ti:Sa regenerative amplifier (Spectra Physics Spitfire, 5 kHz) were frequency doubled in a Type I LBO crystal to produce ~416 nm pulses. The excitation light was split into three equal portions (~20–25 nJ per pulse, ~50 fs FWHM), individually time-delayed, and focused into the sample (700 μM Ab-MPTS complex in 1× PBS, pH 7.4) contained in a spinning cell with a path length of 250 μm. The 3PEPS signals were detected in two phase-matching directions k_1-k_2+k_3 and -k_1+k_2+k_3 with two silica photodiodes using lock-in amplification. The coherence period τ (time delay between first and second pulse) was scanned from –150 fs to 150 fs with a fixed value for the population period *T* (time delay between second and third pulse). The average shift from zero of the temporal signal maximum in τ for two phase-matching directions is referred to as the peak shift for a given *T*. Transient grating (TG) experiments were performed by scanning *T* from 0 to 400 ps at τ = 0. The TG signals for MPTS bound to each Ab were fit to multi-exponential decays and are shown in Figure S2. The 3PEPS decays were fit using a model spectral density function, as described previously,[1, 2] and a representative simultaneous least-square fit of absorption spectrum and 3PEPS peak-shift decay for MPTS bound to Ab 10A6 are shown in Figure S3.

Decay-Associated Difference Spectra. Global lifetime analysis of the transient absorption data was performed using OPTIMUS software.[3] The transient absorption signal $S(t, \lambda)$ was fit to a sum of exponentials:

$$S(t,\lambda) = \sum_{i=0}^{n} A_i(\lambda)\exp\left(-t/\tau_i\right)$$

The pre-exponential factors $A_i(\lambda)$ from the fits were plotted against wavelength to generate decay-associated difference spectra (DADS). A positive feature corresponds to a signal decay with the respective time constant, and negative features indicate growth. The DADS spectra for MPTS bound to Ab 5D11 are shown in Figure S4.

Photophysics of Ab-MPTS Complex. As described in the main text, the MPTS titrations (Figure S5-S7) clearly indicated that the broadening of absorption spectra of MPTS bound to Abs is not due to the formation of H-type dimers or higher aggregates. In addition, TG experiments confirmed that the observed fluorescence quenching is not due to a fast radiationless decay of the fluorescent S_1 state of MPTS back to the ground state but rather due either to the direct excitation of a long-lived, non-fluorescent excited state or to a fast excited-state population transfer from the originally excited, fluorescent S_1 state of MPTS to a secondary, non-fluorescent excited state (Figure S8).

We also performed pump-probe transient absorption (TA) experiments to test for evidence of excited-state population transfer. An excited-state population transfer from the initial to a secondary excited state should lead to spectral changes in induced absorption and stimulated emission while leaving the ground state-bleach unaffected. Figure 3 (main text) shows the normalized transient absorption spectra of MPTS bound to Ab 5D11 at 0.2 ps, 1 ps and 50 ps after excitation in the spectral range of the MPTS ground-state bleach (~400 nm), stimulated emission (430 – 450 nm), and S_1-S_n induced absorption (500 – 600 nm). The spectra are nearly identical except for a slight narrowing of the feature around 525 nm and a slight broadening of the shoulder at 590 nm. Similar small spectral changes occur for MPTS free in solution (Figure 3, main text), where they have been assigned to solvation dynamics.[4] As MPTS is shielded from solvent when bound to the Ab, based on crystal structure, we assign the small spectral shifts in the TA spectra of the MPTS-Ab complexes to protein reorganization. Furthermore, global analysis of the TA data using the method of DADS, required only two decay components to fit the data (Figure S4): a low-amplitude 5 ps component, which reflects the small spectral shifts associated with protein reorganization, and a 1.5 ns component that reflects the excited-state lifetime, in good agreement with the TG experiments. Thus, the TA experiments provide no evidence of an excited-state population transfer. Furthermore, the absence of a stimulated emission signal for the MPTS-Ab complexes at early delay times (Figure S9) argues against fluorescence quenching via excited-state population transfer and for the direct excitation of a nonfluorescent excited state. Given the instrument cross-correlation of ~200 fs for the TA experiment, we expect to be able to detect a ~50 fs process after deconvolution of the instrument response, and as a result, any masked process would have to be complete within ~50 fs.

Crystallization, X-ray Data Collection, Processing, and Model Refinement. 10A6 IgG in 0.1 M sodium acetate, pH 5.5, was cleaved with 2% activated papain; after 4 h, 200 mM iodoacetamide was added to stop the reaction. The cleaved Fab/IgG mixture was applied to a protein A column, and the unliganded Fab was further purified by size exclusion chromatography on a S200 16/60 column (GE) in 20 mM Tris, 150 mM NaCl, pH 7.5. Fab was then mixed with MPTS in a 1:5 molar ratio. Crystals of the complex were grown in sitting drops with a well solution of 1.6 M ammonium sulfate, 0.1 M acetate, pH 5.1, 20% glycerol. Crystals were cryoprotected by brief immersion in the well solution augmented with glycerol to a final concentration of 30%. X-ray diffraction data were collected at APS 23-ID-D using an ADXV m300 CCD detector and processed with HKL-2000.[5] Scaling of the data indicated an apparent space group of either $P3_112$ or $P3_212$, while examination of the native Patterson map showed peaks at u=1/3, v=2/3, w=0 and u=2/3, v=1/3, w=0 with a height 32% of the origin peak. As expected from the observed Patterson peaks, reflections with indices -h+k=3n were systematically stronger than their neighboring reflections. Molecular replacement (MR) was initially carried out in space groups $P3_112/P3_212$ using the individual variable and constant domains from Fab 29G12 (PDB entry 1MEX) as models, with Phaser V 2.1.4.[6] Matthews coefficient calculations suggested either 3 Fabs (V_m= 3.13A^3/Da) or 4 Fabs (V_m=2.35 A^3/Da) in the asymmetric unit. However, no more than 5 domains (2 ½ Fabs) could be successfully placed, but an intact Fab with the correct elbow angle could be derived from

the incomplete solution, and subsequent MR runs were carried out with that intact Fab model. Three Fabs could then be placed in the $P3_212$ cell, but steric clashes were evident, and rigid body refinement failed due to atoms on special positions. MR was then carried out in spacegroups $P3_1/P3_2$ and a solution with 6 Fabs was found in $P3_2$; however, refinement with Phenix[7] stalled with R_{free} values of about 33%. We then carried out MR in space group P1 and subsequently tested different space group choices with Zanuda.[8] The results from Zanuda confirmed that the correct space group was indeed $P3_2$, but revealed that, in addition to the correct crystallographic origin, there were two pseudo-origins for this crystal form. Choosing the correct origin finally led to better refinement results. Because non-crystallographic translational symmetry can mask intensity-based twinning indicators, we were not sure whether these crystals were also twinned. The Yeates-Padilla L-test[9] indicated a small degree of twinning might be present with a mean |L| of 0.47. R versus R statistics[10] for twin operator -k, -h, -l, gave an R^{obs}twin = 0.028 and R^{calc}twin= 0.279, indicative of partial to perfect twinning. Finally, twin refinement improved R-values by about 4% compared to refinement without twinning. Thus, our final model is refined as a twinned crystal, with twin fraction of 0.49. Final R_{work} and R_{free} values were 22.1% and 25.2%. Final data collection and refinement statistics are listed in Table S1.

Table S1. X-ray Data Collection and Refinement Statistics for Fab 10A6-MPTS

Beamline	APS 23-ID-D
wavelength (Å)	1.03318
resolution (Å)[a]	44.8–2.6 (2.64–2.6)
space group	$P3_2$
twin law	-k,-h,-l
unit cell (Å)	186.5, 186.5, 89.9
Unit cell (°)	90., 90., 120.
total reflections	621,989 (31,441)
unique reflections	106,209 (5329)
multiplicity	5.9 (5.7)
completeness (%)	99.9 (100.0)
mean (I/σ_I)	20.0 (1.0)
R_{merge}[b] (%)	9.8 (197)
R_{meas}[c] (%)	10.8 (216)
R_{pim}[d] (%)	4.5 (91)
$CC_{1/2}$[e] (%)	87.9 (38.4)
R_{work} (%)	21.9(34.1)
R_{free} (%)	25.9(32.8)
no. of reflections used in refinement (work/free)	101,010(5164)
no. protein atoms	19,310
no of waters	148
no. of protein residues	2701
RMS (bonds)	0.003
RMS (angles)	0.653
Ramachandran favored, allowed, outliers (%)	94.75, 5.17, 0.08
Clashscore[f]	2.1
Wilson B ($Å^2$)	60
average B factor ($Å^2$)	
Protein	92
MPTS	63
Water	50
PDB entry	6M87

[a]Numbers in parentheses are for highest resolution shell
[b]$R_{merge} = \Sigma_{hkl} \Sigma_{i=1,n} |I_i(hkl) - \langle I(hkl) \rangle| / \Sigma_{hkl} \Sigma_{i=1,n} I_i(hkl)$
[c]$R_{meas} = \Sigma_{hkl} \sqrt{(n/n-1)} \Sigma_{i=1,n} |I_i(hkl) - \langle I(hkl) \rangle| / \Sigma_{hkl} \Sigma_{i=1,n} I_i(hkl)$
[d]$R_{pim} = \Sigma_{hkl} \sqrt{(1/n-1)} \Sigma_{i=1,n} |I_i(hkl) - \langle I(hkl) \rangle| / \Sigma_{hkl} \Sigma_{i=1,n} I_i(hkl)$
[e]$CC_{1/2}$ = Pearson Correlation Coefficient between two random half datasets
[f]Number of unfavorable all-atom steric overlaps ≥ 0.4Å per 1000 atoms

Nucleotide sequence of Ab

>10A6-H

ctcgagtctggacctgagctggtgaagcctggcgcttcagtgaagatatcctgcaaggcttctggttactcattcactgactacaacatga
actgggtgaagcagagcaatggaaagagccttgagtggattggagtaattaatcctaactctggtactactaactacaaccagaagttcaa
ggacaaggccacattgactgtagaccaatcttccagcacagcctacatgcaactcaacagcctgacatctgaggactctgcagtctattac
tgtgccaggggggggggattccgacgcggatttgactcctggggccaaggcaccacggtcacc

>10A6-L

gagctcgtgctcacccagtctccagcaattatgtctgcatctccaggggagaaggtcaccatgacctgcagtgccagttcaagtgtaagtt
acgtgcattggtaccagcagaagtcaggcacctcccccaaaagatggatttatgacacatccaaactggcttctggagtccctgctcgctt
cagtggcagtgggtctgggacttcttactctctcacaatcagcagcatggaggctgaagatgctgccacttattactgccatcagtggagg
actaacccacccacgttcggtgctgggaccaagctt

>5D11-H

ctcgagtctggacctgagctggtgaagcctggcgcttcagtgaagatatcctgcaaggcttctggttactcattcactgactacaacatga
actgggtgaagcagagcagtggaaagagccttgagtggattggactaattaatcctaactatggtactactaactacaaccagaagttcaa
gggcaaggccacattgactgtagaccaatcttccaacacagcctacatgcaactcaacagcctgacatctgaggactctgcagtctattac
tgtgccaggggggggggattccgacgcggatttgactcctggggccaaggcaccacggtcacc

>5D11-L

gagctcgtgctcacccagtctccagcaattatgtctgcatctccaggggagaaggtcaccatgacctgcagtgccagctcaagtgtaagtt
acatgcattggtaccagcagaagtcaggcacctcccccaaaagatggatttatgacacatccacactggcttctggagtccctgctcgctt
cagtggcagtgggtctgggacctcttattctctcacaatcagcagcatggaggctgaagatgctgccacttatcactgccatcagtggagg
actaacccacccacgttcggtgctgggaccaagctt

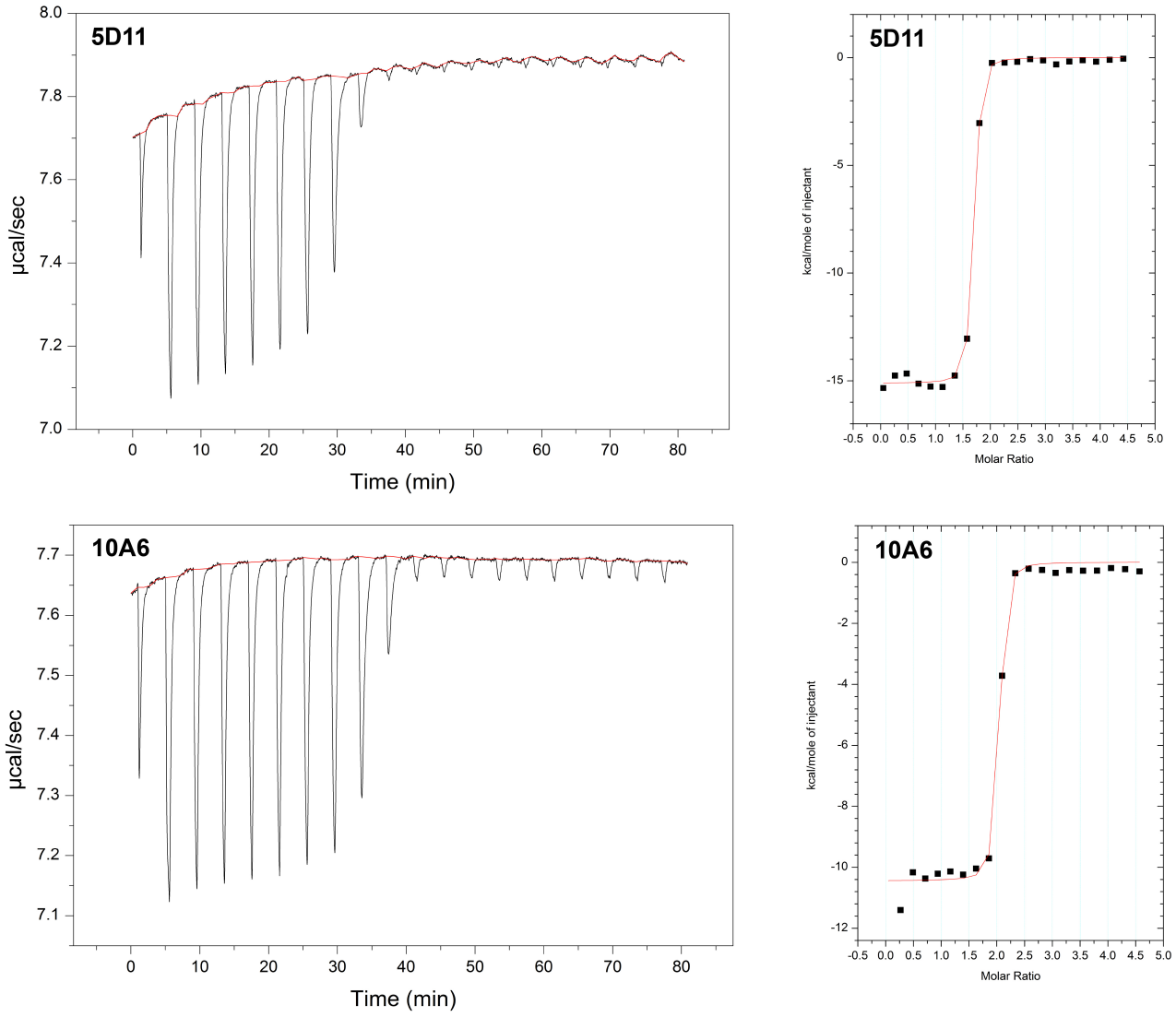

Figure S1. Representative raw ITC data and binding isotherm of 5D11 and 10A6 at 25 °C.

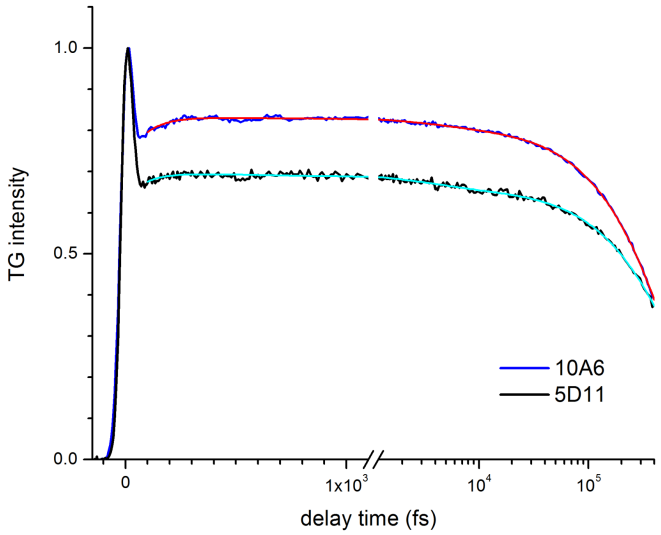

Figure S2. TG signals of MPTS bound to Ab 5D11 (black line) and Ab 10A6 (blue line). Also shown are multi-exponential fits for delay times larger than 100 fs (cyan line, 5D11; red line, 10A6).

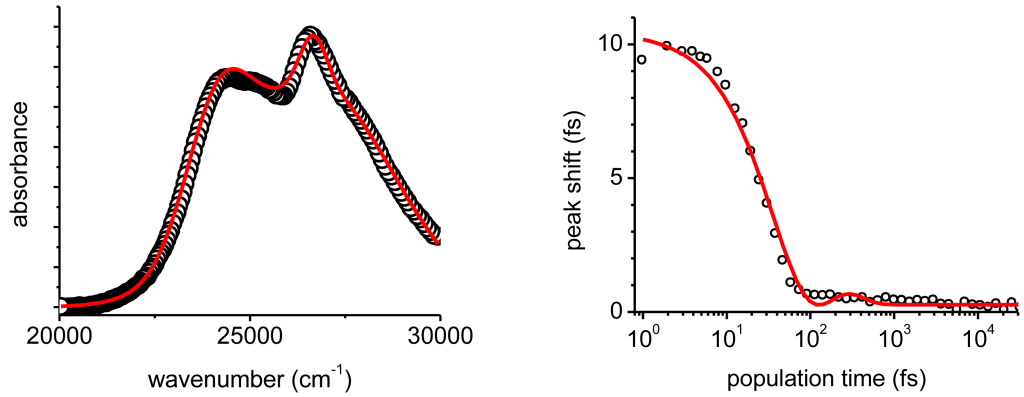

Figure S3. Simultaneous fit of absorption spectrum (*left*) and 3PEPS peak-shift decay (*right*) for MPTS bound to Ab 10A6.

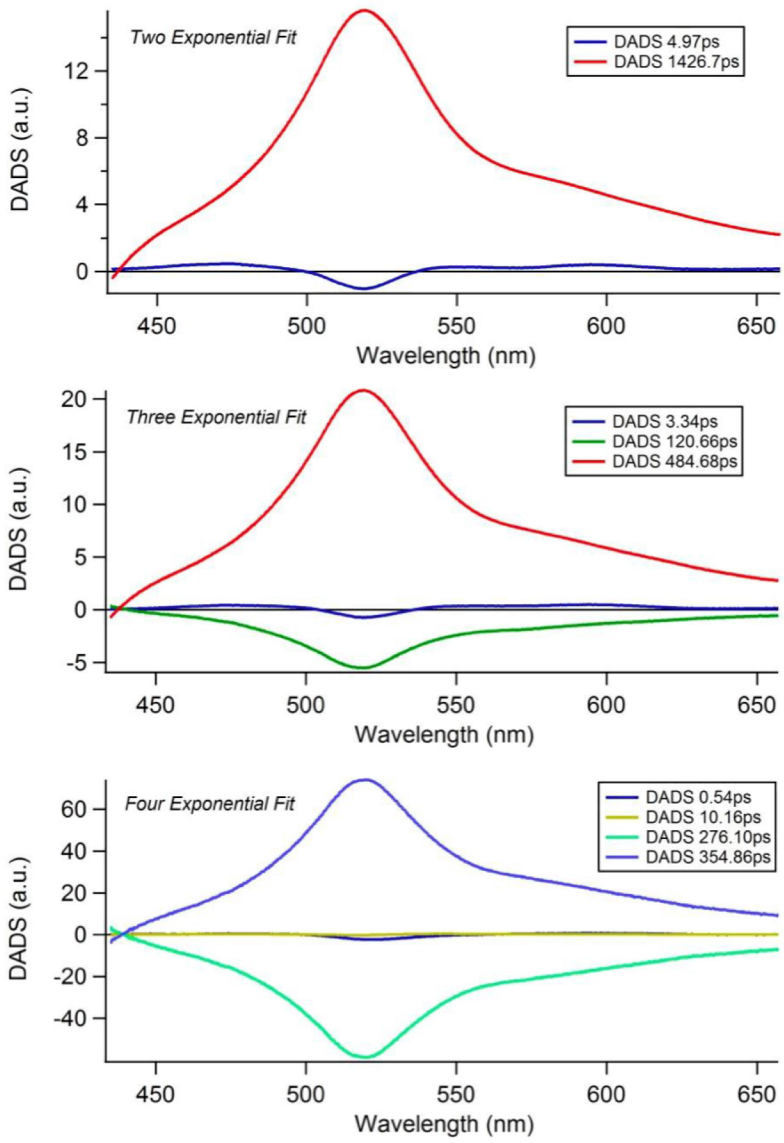

Figure S4. DADS analysis for 5D11-MPTS complex using two, three, or four exponential functions. The time constants of the exponential decay components are given in the panel legends.

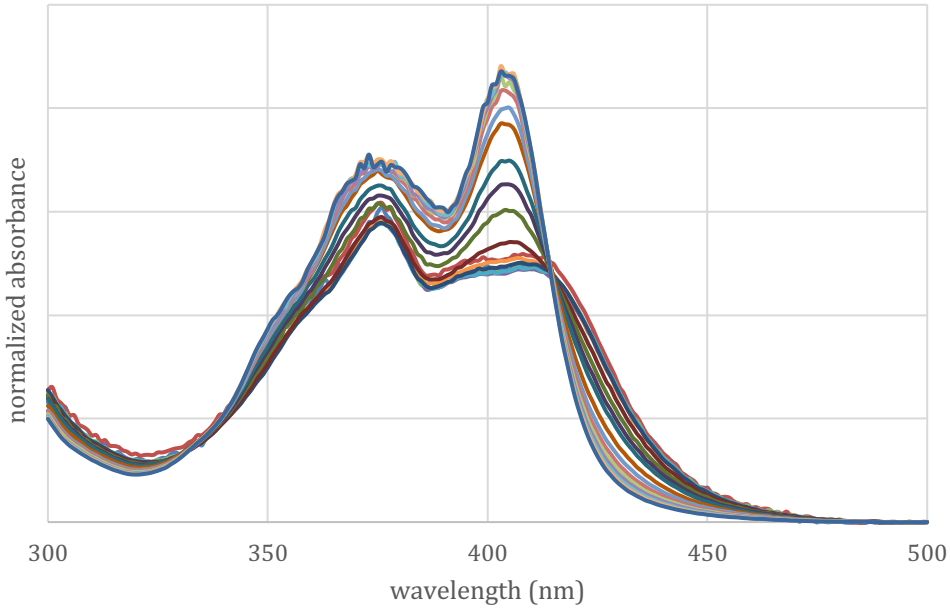

Figure S5. Absorption spectra divided by MPTS concentration for titration of a 27 μM binding site concentration (13.5 μM IgG concentration) of Ab 5D11 with increasing amount of MPTS.

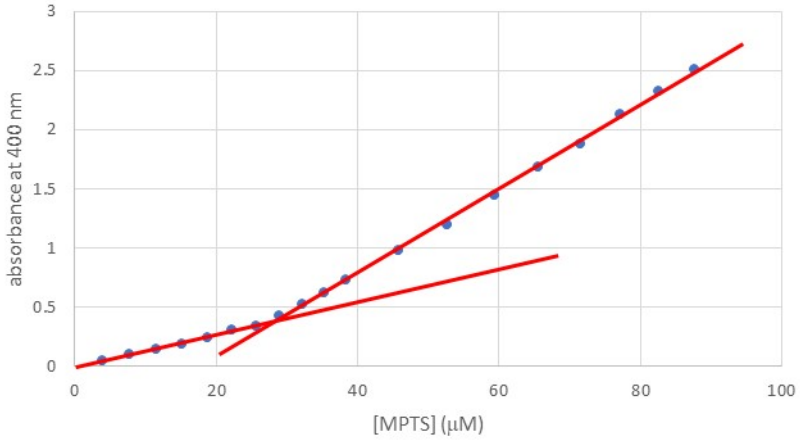

Figure S6. Absorbance at 400 nm as a function of MPTS concentration in a 27 μM solution of Ab 5D11.

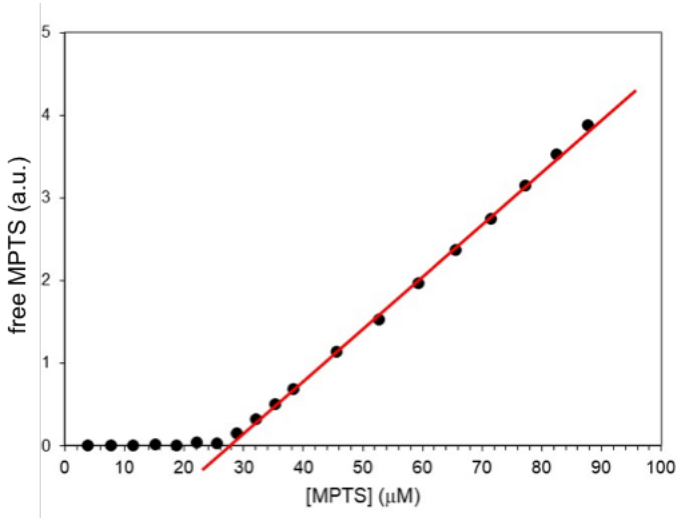

Figure S7. Deconvolution of the absorption spectra of MPTS at varying concentration in a 27 μM solution of Ab 5D11.

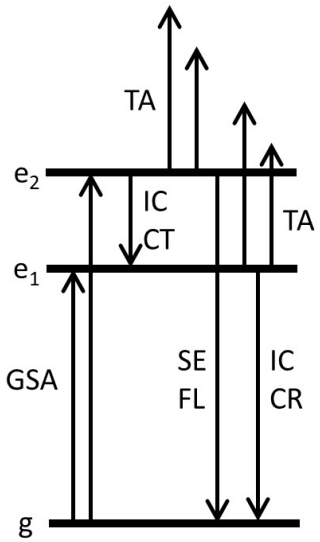

Figure S8. Three-state model of the MPTS-Ab complex (g, ground state; e_1, lowest-energy excited state; e_2, second-lowest excited state; GSA, ground-state absorption; TA, transient absorption; SE, stimulated emission; IC, internal conversion; FL, fluorescence; CT, charge transfer; CR, charge recombination).

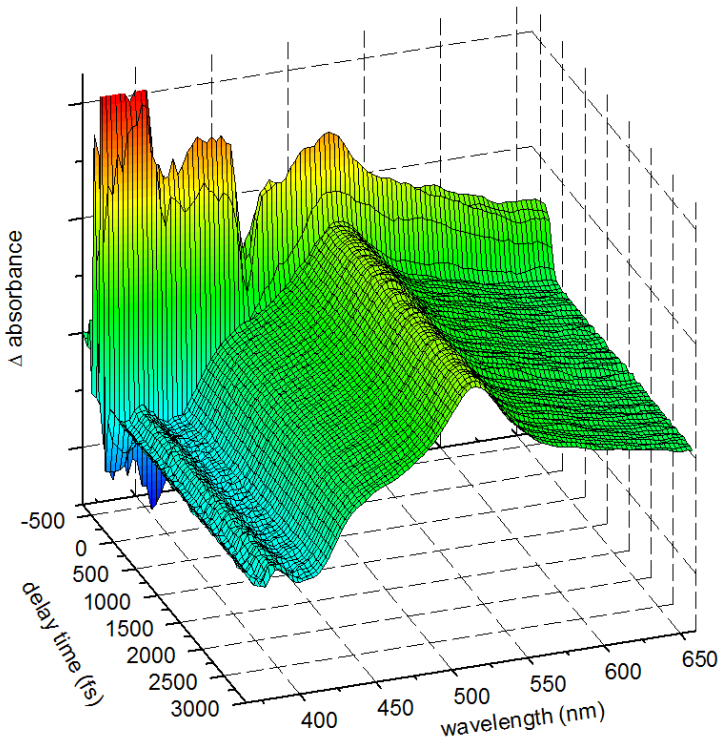

Figure S9. Transient absorption spectra of the 5D11-MPTS complex (25 fs step size).

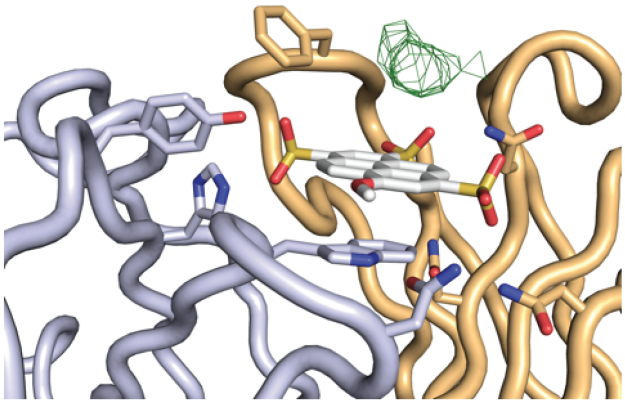

Figure S10. Difference electron density map for Phe^{H}98. Difference (F_o-F_c) map contoured at 2σ is shown in green.

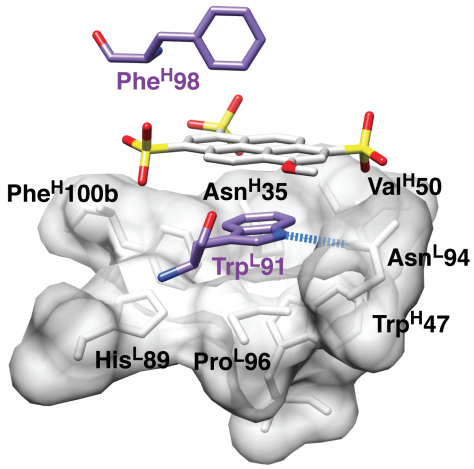

Figure S11. Packing and H-bonding interactions of Trp^{L}91 within the Ab binding pocket, with the side chain of Phe^{H}98 in the T-shaped conformation also shown.

References

(1) Jimenez, R., Case, D. A., and Romesberg, F. E. (2002) Flexibility of an antibody binding site measured with photon echo spectroscopy, *J. Phys. Chem. B 106*, 1090–1103.

(2) Adhikary, R., Yu, W., Oda, M., Walker, R. C., Chen, T., Stanfield, R. L., Wilson, I. A., Zimmermann, J., and Romesberg, F. E. (2015) Adaptive mutations alter antibody structure and dynamics during affinity maturation, *Biochemistry 54*, 2085–2093.

(3) Slavov, C., Hartmann, H., and Wachtveitl, J. (2015) Implementation and evaluation of data analysis strategies for time-resolved optical spectroscopy, *Anal. Chem. 87*, 2328–2336.

(4) Spry, D. B., Goun, A., and Fayer, M. D. (2007) Deprotonation dynamics and stokes shift of pyranine (HPTS), *J. Phys. Chem. A 111*, 230–237.

(5) Otwinowski, Z., and Minor, W. (1997) Processing of X-ray diffraction data collected in oscillation mode, *Methods Enzymol. 276*, 307–326.

(6) McCoy, A. J., Grosse-Kunstleve, R. W., Adams, P. D., Winn, M. D., Storoni, L. C., and Read, R. J. (2007) Phaser crystallographic software, *J. Appl. Crystallogr. 40*, 658–674.

(7) Afonine, P. V., Grosse-Kunstleve, R. W., Echols, N., Headd, J. J., Moriarty, N. W., Mustyakimov, M., Terwilliger, T. C., Urzhumtsev, A., Zwart, P. H., and Adams, P. D. (2012) Towards automated crystallographic structure refinement with phenix.refine, *Acta Cryst. Sect. D, Biol. Cryst. 68*, 352–367.

(8) Lebedev, A. A., and Isupov, M. N. (2014) Space-group and origin ambiguity in macromolecular structures with pseudo-symmetry and its treatment with the program Zanuda, *Acta Cryst. Sect. D, Biol. Cryst. 70*, 2430–2443.

(9) Padilla, J. E., and Yeates, T. O. (2003) A statistic for local intensity differences: robustness to anisotropy and pseudo-centering and utility for detecting twinning, *Acta Crystallogr. D Biol Crystallogr. 59*, 1124–1130.

(10) Lebedev, A. A., Vagin, A. A., and Murshudov, G. N. (2006) Intensity statistics in twinned crystals with examples from the PDB, *Acta Crystallogr. D Biol Crystallogr. 62*, 83–95.